Journal of ELECTRONIC MATERIALS, Vol. 47, No. 9, 2018
https://doi.org/10.1007/s11664-018-6443-y
© 2018 The Minerals, Metals & Materials Society

CrossMark

Investigation of the Growth Process of Continuous Monolayer MoS_2 Films Prepared by Chemical Vapor Deposition

WENZHAO WANG,[1] XIAOXIAO CHEN,[1] XIANGBIN ZENG,[1,4] SHAOXIONG WU,[1] YANG ZENG,[1] YISHUO HU,[1] SUE XU,[2] GUANGTONG ZHOU,[2] and HONGXING CUI[3]

1.—School of Optical and Electronic Information, Huazhong University of Science and Technology, Wuhan 430074, China. 2.—China-Eu Institute for Clean and Renewable Energy, Huazhong University of Science and Technology, Wuhan 430074, China. 3.—Tashan Industry Zone, Meilin Street, Ninghai County, Ningbo City, China. 4.—e-mail: eexbzeng@163.com

Recently, great efforts have been devoted to study of molybdenum disulfide (MoS_2), particularly monolayer MoS_2 semiconductor thin films, due to its excellent electrical and optical properties. Direct growth of continuous monolayer MoS_2 films by ambient-pressure chemical vapor deposition is reported herein. Optical microscopy, Raman spectroscopy, photoluminescence spectra (PL), atomic force microscopy, x-ray photoelectron spectroscopy (XPS), and high-resolution transmission electronic microscopy were used to characterize the electronic and structural properties of the films, demonstrating that the MoS_2 films grown on silicon dioxide/silicon (SiO_2/Si) substrate with spatial size on micron scale were high quality, single crystal, continuous, and monolayer. Raman and PL mapping were performed to confirm the uniformity of the monolayer MoS_2 films. The morphological variation of the MoS_2 films after different reaction times was observed by optical microscopy and scanning electron microscopy, revealing the growth process and thus helping to understand that the growth mechanism during synthesis of continuous large-area films depends on the distribution of the reactive intermediate molybdenum oxide (MoO_{3-x}) due to its lower saturation vapor density. Back-gated transistors based on MoS_2 films were fabricated, exhibiting current on/off ratio of $\sim 10^4$ and subthreshold swing (SS) of 0.44 V dec^{-1}. This work contributes to synthesis of large-area continuous films, thus paving the way for future scaled-up fabrication of MoS_2 electronic devices.

Key words: Molybdenum disulfide, chemical vapor deposition, continuous films, growth process

INTRODUCTION

Molybdenum disulfide (MoS_2), a member of the transition-metal dichalcogenides (TMDCs), has attracted much attention because of its favorable optical, electronic, mechanical, and chemical properties.[1–5] As a novel two-dimensional material, compared with gapless semimetal graphene,[6] MoS_2 is promising for optoelectronic applications not only because of its intrinsically *n*-type semiconducting nature but also its layer-dependent bandgap,[7,8] which shows an indirect to direct transition when decreasing the number of layers from bulk to a monolayer, covering the energy range from 1.20 eV to 1.85 eV. The direct bandgap of single-layer MoS_2 also results in a strong photoluminescence phenomenon. Besides, monolayer MoS_2 shows favorable carrier mobility (100 $cm^2\ V^{-1}\ s^{-1}$ to 400 $cm^2\ V^{-1}\ s^{-1}$)[9] and good chemical sensitivity, enabling wide applications in field-effect transistors (FETs),[10] photosensors,[11] chemical gas sensors,[12] photovoltaic cells,[3] etc. In particular, it is a

(Received November 3, 2017; accepted June 9, 2018; published online June 26, 2018)

suitable candidate for use in flexible electronics such as displays, wearable devices, etc., due to its high mechanical strength.[13,14]

Among many MoS_2 growth techniques, such as micromechanical exfoliation,[15,16] physical vapor deposition,[17] liquid exfoliation,[18] and chemical vapor deposition (CVD), the latter is the most promising technology because it can prepare high-quality films.[19–23] Recently, controllable synthesis of single- and few-layer MoS_2 on silicon dioxide (SiO_2) substrates using predeposition of molybdenum (Mo) film followed by CVD was realized.[24] The results demonstrated that the size and thickness of the MoS_2 are inherited from the nature of the predeposited Mo. However, the balance between adatom mobility and surface evaporation gives rise to limited sizes of as-grown films and low yield of monolayer films. Another group synthesized millimeter-scale MoS_2 sheets with seeds at the center of each MoS_2 star- or irregular-shaped grain using a seeding-assisted CVD method.[19] It is worth noting that the smoothness of the grains and grain boundaries plays an important role in the electrical properties of MoS_2 films, with direct growth of triangular-shaped MoS_2 on silicon dioxide/silicon (SiO_2/Si) substrate with smoother surface therefore being desirable. More recently, Dumcenco et al. described epitaxial CVD growth of centimeter-scale uniform monolayer MoS_2 on sapphire.[25] This kind of MoS_2 film must be transferred to SiO_2/Si chips for use in FETs, but this transfer procedure can introduce contamination and/or degradation.[26] Moreover, the growth mechanism of continuous MoS_2 thin films for device applications has not yet been clarified.

Direct growth of continuous large-area monolayer MoS_2 on SiO_2/Si substrate, which would enable seamless device integration, is badly needed. In the work presented herein, we studied direct synthesis of continuous large-area monolayer MoS_2 films on SiO_2/Si substrate via ambient-pressure CVD. Various characterization techniques including Raman spectroscopy, photoluminescence spectroscopy (PL), atomic force microscopy (AFM), high-resolution transmission electron microscopy (HRTEM), and x-ray photoelectron spectroscopy (XPS) were applied to determine the quality of the films. Optical microscopy and scanning electron microscopy (SEM) were used to reveal the morphology of the as-grown MoS_2 films after different reaction times. The morphological variation of the MoS_2 films after different reaction times revealed the growth process, thus helping to optimize the growth conditions and verifying the proposed growth mechanism for MoS_2 thin films. To confirm the electronic properties of such continuous large-area monolayer MoS_2 films, back-gated transistors based on continuous large-area MoS_2 films were fabricated, exhibiting on/off ratio of $\sim 10^4$ and subthreshold swing (SS) of ~ 0.44 V dec^{-1}.

EXPERIMENTAL PROCEDURES

Synthesis of Continuous MoS_2 Thin Films

Figure 1 illustrates the synthesis of MoS_2 thin films. The experimental setup used throughout this study is presented schematically in Fig. 1a. The substrate, viz. crystalline silicon coated with 300 nm of SiO_2, was cleaned sequentially in acetone, alcohol, and deionized (DI) water. Molybdenum trioxide (MoO_3, 99.99%; Alfa) and solid sulfur (99.99%, Aladdin) were used as precursor and reactant, respectively, to synthesize MoS_2 thin films by CVD at atmospheric pressure. A quartz boat was used to place sulfur (S) powder (0.5 g), being located in the upstream cold zone of the 2-inch-diameter quartz tube. MoO_3 powder was sandwiched between two face-to-face substrates. A substrate carrying MoO_3 powder (3 mg) was placed in the middle of the heating zone, while the other substrate was placed face-down above the MoO_3 powder. During the growth process, the furnace was gradually heated up to 800°C at rate of about 15°C min^{-1} and held there for several minutes. During the whole reaction, nitrogen flow at 80 sccm was applied. After that, the furnace was cooled naturally to room temperature. Nitrogen was applied as carrier gas to bring S vapor from upstream to the reaction zone and protect the CVD system from oxygen contamination. The material was synthesized on the substrate placed face-down above the MoO_3 powder. A

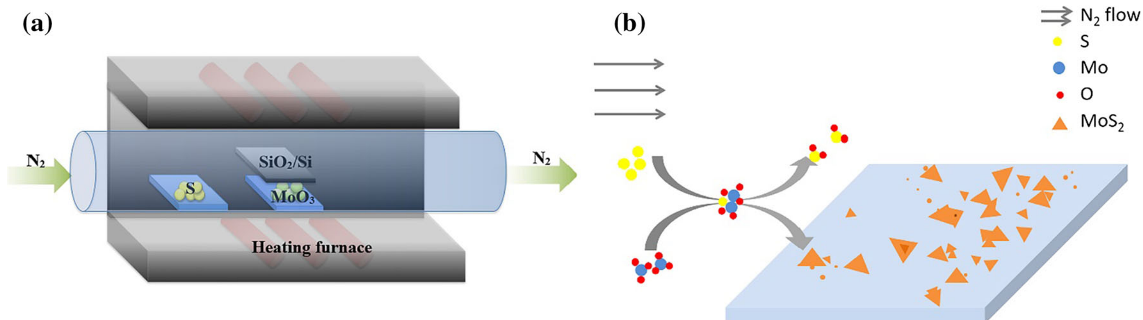

Fig. 1. Synthesis of MoS_2 thin layers: (a) experimental setup of CVD system and (b) schematic view of MoS_2 film growth.

detailed schematic illustration of the formation of MoS_2 thin films is presented in Fig. 1b: evaporated MoO_3 is gradually sulfurated by sulfur vapor to produce partially sulfurated reactive intermediate, and further sulfurated into MoS_2 nanoparticles, which diffuse to the substrate surface to form MoS_2 films.

Characterization of As-Grown MoS_2 Films

We used an HR 800 (HORIBA Jobin–Yvon) spectrometer to obtain Raman spectra and carry out Raman mapping. This spectrometer was equipped with a neodymium-doped yttrium aluminium garnet (Nd-YAG) laser at 532 nm as excitation source, focused on the surface of the ultrathin MoS_2 monolayer films through a 100× objective with power of 5 mW. PL measurements and PL mapping were also carried out using an HR 800 (HORIBA Jobin–Yvon) spectrometer under excitation by a neodymium-doped yttrium aluminium garnet (Nd-YAG) laser at 532 nm. The surface morphology and microstructure of MoS_2 were examined by scanning electron microscopy (FEI, Nova Nano 450). Optical microscopy (VHX-1000) and atomic force microscopy (Bruker Dimension Icon) were also conducted to observe the surface morphology and thickness of the as-deposited films in tapping mode. High-resolution transmission electron microscopy (Tecnai G2 F30, FEI and JEM 2100, JEOL) was employed to investigate the crystal structure of the MoS_2 thin films. X-ray photoelectron spectroscopy (AXIS-ULTRA DLD-600 W) was applied to investigate the sample composition.

Device Fabrication and Characterization

Back-gated monolayer MoS_2 FETs were fabricated directly on the SiO_2/Si substrates without any transfer procedure using electron-beam lithography followed by electron-beam deposition of metal titanium/gold (Ti/Au) thin films (5 nm/15 nm thick) followed by a lift-off process. The patterned Ti/Au formed source and drain electrodes on the MoS_2 films. We used a Keithley 4200S semiconductor parameter analyzer to measure the FET characteristics then calculated the SS and current on/off ratio for the MoS_2 FETs. The SS of these MoS_2 devices was estimated using the following equation:

$$\mathrm{SS} = \left(\frac{\mathrm{d}\log I_{\mathrm{DS}}}{\mathrm{d}V_{\mathrm{GS}}}\right)^{-1}.$$

RESULTS AND DISCUSSION

Optical microscopy images were used to characterize the morphological variation of the as-grown MoS_2 films after different reaction times of 5 min, 8 min, 10 min, and 15 min (Fig. 2a–d). For reaction time of 5 min, the synthesized material was small dispersed triangle-shaped MoS_2 domains (Fig. 2a). When the reaction time was increased to 8 min, the

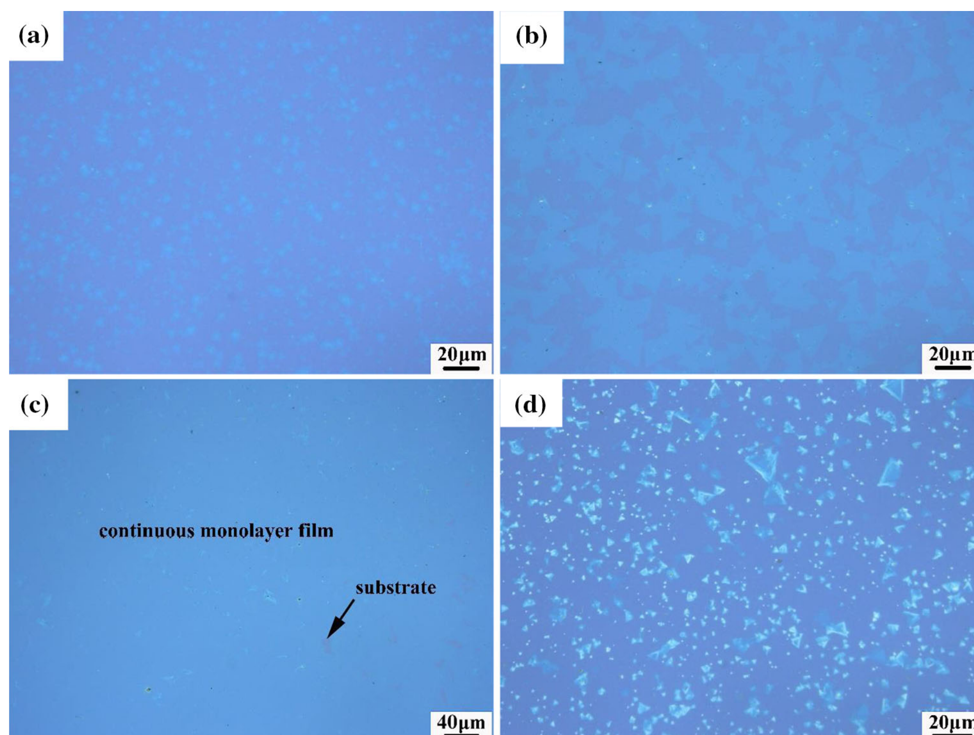

Fig. 2. Optical microscopy images showing morphology after different growth times: (a) 5 min, (b) 8 min, (c) 10 min, and (d) 15 min.

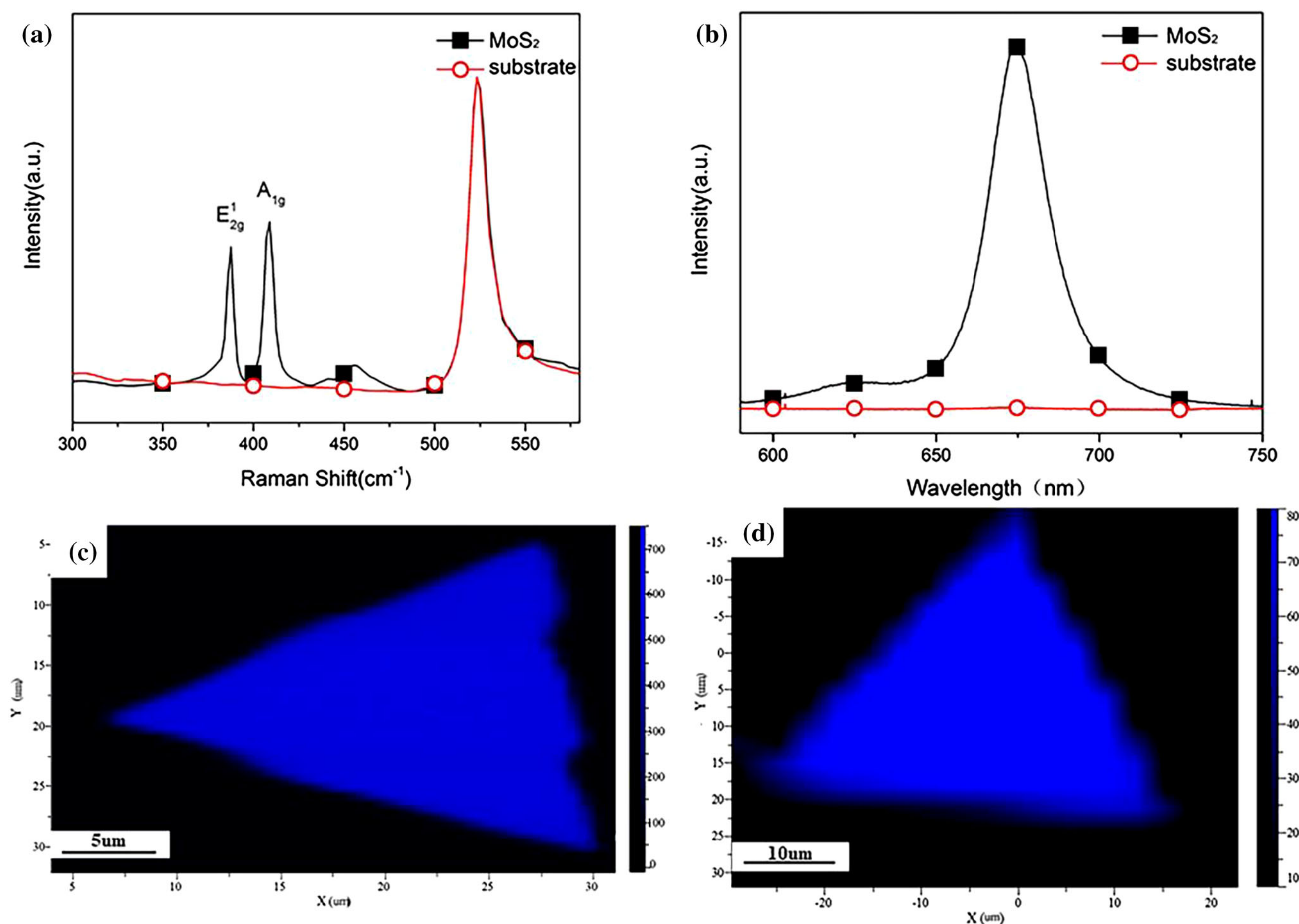

Fig. 3. Spectroscopic characterization of MoS_2 films: (a) Raman spectra of monolayer MoS_2 on SiO_2/Si substrate, (b) PL spectrum of monolayer MoS_2 films, (c) Raman map of monolayer MoS_2 domain, showing the spatial variation of the intensity of the Raman signal, and (d) PL map of monolayer MoS_2 domain. Both Raman and PL experiments were performed in a confocal spectrometer using excitation by a laser at 532 nm.

triangle-shaped domains became larger, while some of them meet and became connected (Fig. 2b). In Fig. 2c the MoS_2 domains have grown into a continuous film at reaction time of 10 min. When the reaction time reached 15 min, the synthesized material was formed of separate domains that were smaller and thicker (Fig. 2d). Based on the morphology of the synthesized material after different reaction times, the MoS_2 film growth process was clarified. Initially, the synthesized material was formed of small triangle-shaped domains scattered randomly on the surface of the substrate (Fig. 2a). Note that, when the reaction time was increased to 8 min (Fig. 2b), MoO_3 reacted with S to produce MoS_2 constantly, and the MoS_2 domains deposited on the substrate continued to grow larger and interconnect with one another. Then, the larger triangle-shaped domains extended to form a continuous film on the substrate when the reaction time reached 10 min. Comparing the color of the film with that of the substrate (indicated by a black arrow in Fig. 2c) revealed that the film showed complete and smooth surface coverage, mainly because the MoS_2 film tended to grow parallel to the surface of the substrate, forming seamless interconnection, rather than overlapping in the direction perpendicular to the substrate surface. Also, the dimension of the continuous film was up to micron scale (with lateral size above 200 μm). However, when the growth time was increased further to 15 min (Fig. 2d), the MoS_2 crystals become smaller and thicker; insufficient precursor in the reaction system may explain such growth arrest of the MoS_2, while as-deposited MoS_2 on the substrate may evaporate at high temperature and flow away with the carrier gas.

Raman spectroscopy was applied to probe the structure and crystalline quality of the MoS_2 films. Two characteristic Raman vibration modes can be seen in the spectrum in Fig. 3a; the peak corresponding to crystalline silicon at around 520 cm^{-1} was used for wavelength calibration. The E^1_{2g} peak located at around 387.8 cm^{-1} is attributed to the in-plane vibration mode, associated with vibration of two S atoms relative to a Mo atom in the opposite direction, while the out-of-plane vibration mode peak A_{1g} is located close to 408.5 cm^{-1}, resulting from vibration of two S atoms in the direction

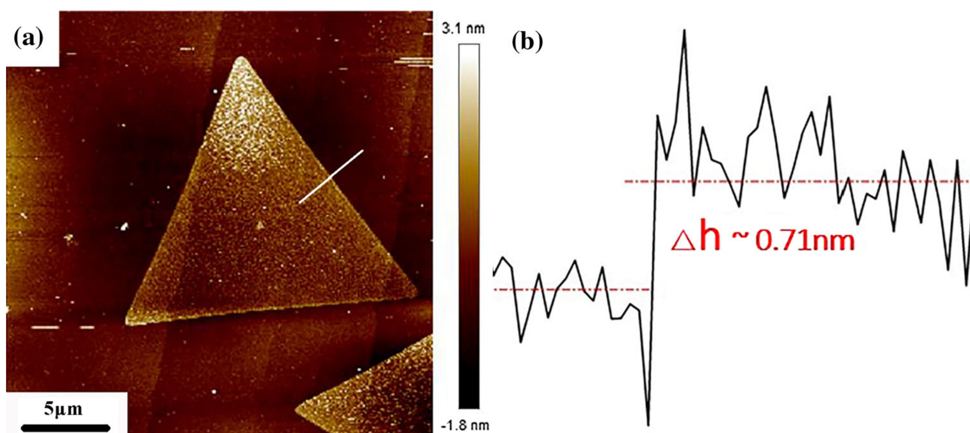

Fig. 4. (a) AFM image of one MoS_2 domain on the substrate. (b) Height profile taken along the white line in (a).

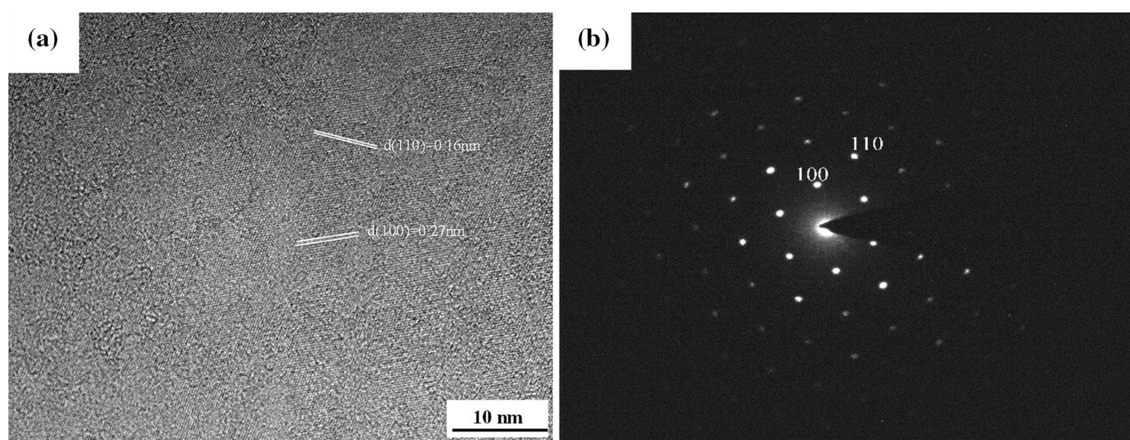

Fig. 5. HRTEM characterization of monolayer MoS_2 film: (a) high-resolution TEM image of MoS_2 film on copper grid and (b) corresponding SAED pattern.

perpendicular to the plane. The frequency difference (ΔK) between E^1_{2g} and A_{1g} can be employed to identify the number of layers in atomic-layered MoS_2,[27] while the full-width at half-maximum (FWHM) of the E^1_{2g} peak is related to the crystalline quality of the film.[20,28] The ΔK characterized in Fig. 3a is 20.7 cm^{-1}, implying that the as-synthesized films were monolayer MoS_2. The E^1_{2g} FWHM of the monolayer MoS_2 was 4.6 cm^{-1}, comparable to values reported for exfoliated monolayers (3.7 cm^{-1}), suggesting good crystalline structure of the synthesized films.[20] We also carried out PL measurements on the films (Fig. 3b), revealing two emission peaks in the spectrum. The peak centered at 625 nm was weakly visible as a shoulder on the strong peak at 675 nm, corresponding to bandgap of MoS_2 of 1.98 eV and 1.83 eV, respectively, being caused by direct excitonic transition from the maxima of the split valence band to the minimum of the conduction band.[29] The PL spectrum of a bare SiO_2/Si wafer is also illustrated in Fig. 3b for comparison. The strong peak at 675 nm in the PL spectra indicates a strong photoluminescence phenomenon. The uniformity of the MoS_2 domains was verified by the Raman and PL mapping results. The color in Raman and PL maps represents the intensity. Figure 3c shows Raman intensity maps for a triangular MoS_2 domain with edge length of 20 μm. Figure 3d shows PL intensity maps for a triangular MoS_2 domain with edge length of 40 μm. Figure 3c and d shows MoS_2 domains with uniform color, suggesting high uniformity of the MoS_2 monolayer.

To further confirm the thickness of the MoS_2 films, we conducted AFM characterization. Figure 4a shows an AFM image of MoS_2 domains on a substrate. The step height image along the white line in Fig. 4a is depicted in Fig. 4b, showing that the thickness of this MoS_2 domain was $\sim$ 0.71 nm, lying in the range for single-layer MoS_2 film on bare substrate (0.6 nm to 0.9 nm)[30] and in good agreement with the previously measured value of 0.62 nm for the S–Mo–S unit.[31] The color of the triangular MoS_2 region was generally uniform, confirming formation of a homogeneous monolayer.

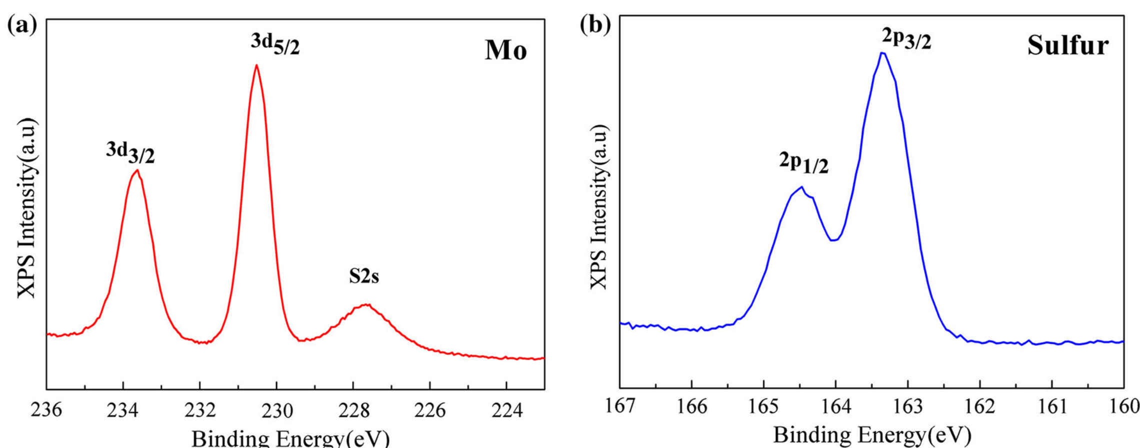

Fig. 6. XPS measurements for binding energies of Mo and S in monolayer MoS_2 films: (a) Mo 3*d* peaks and (b) S 2*p* peaks.

The crystalline structure of the monolayer MoS_2 was obtained by HRTEM. Figure 5a and b shows HRTEM images of MoS_2 films. We transferred MoS_2 films onto copper grid via a poly(methyl methacrylate)-assisted method to prepare samples for HRTEM characterization. Figure 5a shows an HRTEM image of a random area of MoS_2 films. Figure 5b shows the selected-area electron diffraction (SAED) pattern, in which the hexagonal symmetrical diffraction spots suggest the single-crystal nature of the scanned area. The measured lattice fringes are 0.27 nm and 0.16 nm, matching well with (100) and (110) planes of hexagonal-phase MoS_2, indicating that the basal plane of the synthesized thin film is (001); i.e., the *c*-axis of the MoS_2 is perpendicular to the thin film.

XPS was used to examine the elemental composition and bonding of the MoS_2 samples. Figure 6a and b presents high-resolution XPS spectra in the Mo and S region for the MoS_2 films. Figure 6a reveals the presence of two highly intense peaks, separated by 3.1 eV, corresponding to Mo $3d_{3/2}$ at 233.6 eV and Mo $3d_{5/2}$ at 230.5 eV. The shoulder peak at 227.7 eV corresponds to S 2*s* due to the existence of S 2*s* in MoS_2. Peaks corresponding to S $2p_{1/2}$ and S $2p_{3/2}$ orbitals of divalent sulfide ions (S^{2-}) were observed at 164.4 eV and 163.1 eV, respectively, consistent with reported peak positions for MoS_2 crystal.[19,32,33] The $\sim$ 1:2 Mo/S ratio obtained from the integrated peak areas confirms that the MoS_2 crystals had the desired stoichiometry.

SEM was used to observe the morphology of the MoS_2 films after different reaction times. Figure 7a presents a SEM image of the synthesized material grown for reaction time of 5 min, while Fig. 7b shows a magnification of the area marked in Fig. 7a. Figure 7c shows a SEM image of the synthesized material grown for reaction time of 10 min, while Fig. 7d shows a magnification of the area marked in Fig. 7c. The boundary between the synthesized continuous film grown for reaction time of 10 min and the substrate is indicated in Fig. 7e. As shown in Fig. 7a, the synthesized material was formed of small triangle-shaped MoS_2 domains located randomly on the substrate. The orientations of the single-crystal MoS_2 domains were random, mainly because of the amorphous feature of the substrate. As the reaction time was increased to 10 min, the triangle-shaped domains became larger (Fig. 7c) and merged into a continuous film (with lateral size above 200 μm) at the center of the substrate (Fig. 7e). The color of the MoS_2 domains was uniform black, as shown in Fig. 7c and e, indicating that the synthesized material had a smooth surface. The size and distribution of the triangle-shaped MoS_2 crystals in Fig. 7a, c, and e coincide with the optical microscopy images measured above. It is worth noting that there are many isolated zero-dimensional fullerene-like MoS_2 nanoparticles with size of a few hundred nanometers independent of the growth time, as shown in Fig. 7b–e. The nanoparticles near the edge of MoS_2 domains were larger and sparser, as shown in Fig. 7b and e, and large nanoparticles were formed from many small nanoparticles, as shown in Fig. 7d. We also noticed that the MoS_2 films exhibited a clear boundary on the substrate surface (Fig. 7e), mainly because of the lower concentration of reactants at the edge of the substrate when located directly above the Mo precursor. MoS_2 crystals adhered in the form of nanoparticles at the substrate edge while aggregating into a continuous film (with lateral size above 200 μm) at the center of the substrate in Fig. 7e, indicating that the MoO_3 concentration is important for formation of continuous MoS_2 films.

These observations further indicate a growth process in which small nanoparticles merge with one another, then grow into large triangle-shaped domains and finally a continuous film. Besides, they

Fig. 7. SEM characterization of as-grown MoS_2 films for different growth times: (a, b) 5 min and (c–e) 10 min. (b) Magnification of area marked in (a). (d) Magnification of area marked in (c).

also provide a clue regarding the growth mechanism during synthesis of large-area continuous MoS_2 films on SiO_2/Si by CVD method.

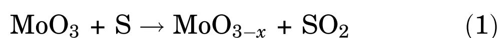

$$MoO_3 + S \rightarrow MoO_{3-x} + SO_2 \quad (1)$$

$$MoO_{3-x} + S \rightarrow MoS_2 + SO_2 \quad (2)$$

The stepwise reaction mechanism during the synthesis is given in Eqs. 1 and 2.[34] Obviously, at the initial stage of the reaction, with increase of the furnace temperature, MoO_3 powder gradually evaporates and reacts with S vapor to produce partially sulfurated molybdenum oxide MoO_{3-x} $(0 < x < 3)$. Then, the MoO_{3-x} vapor reacts with S vapor, resulting in synthesis of MoS_2. The saturation vapor density of MoO_{3-x} is less than that of MoO_3, therefore the MoO_{3-x} vapor flows further than the MoO_3 vapor with the carrier gas and reacts with S to form MoS_2. The saturation vapor density of MoS_2 is the highest among MoO_3, MoO_{3-x}, and MoS_2. The heaviest MoS_2 vapor turns into solid nanoparticles that deposit on the substrate surface, while the precursors and reactive intermediate are taken away by the carrier gas. These initial MoS_2 nanoparticles become nucleation sites. Then the

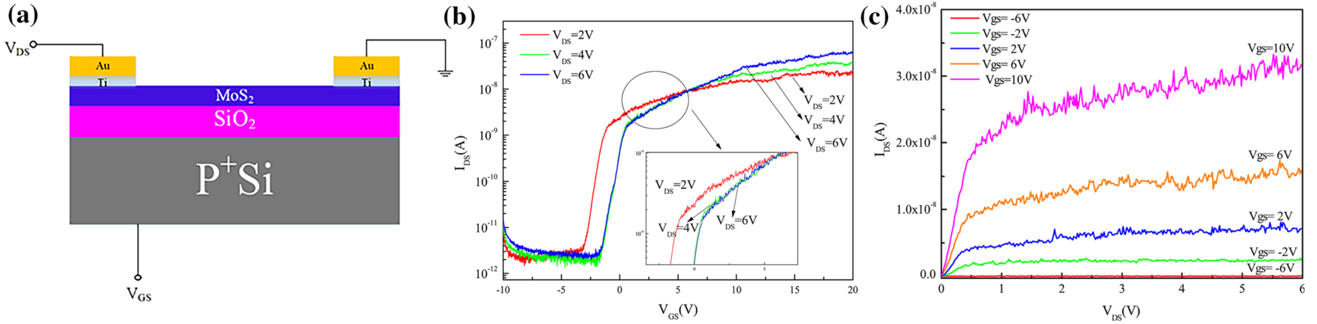

Fig. 8. (a) Schematic diagram of MoS_2-based device. (b) log I_{DS}–V_{GS} curves for as-grown MoS_2 FET at various biases probed in air. (c) I_{DS}–V_{DS} curves for the device in (b) at varied V_{GS} probed in air.

lightest MoO_{3-x} keeps flowing ahead, and finally reacts to form MoS_2 nanoparticles that act as nucleation sites for MoS_2 cluster growth. These nanoparticles merge into a larger area of nucleation sites, compared with the MoS_2 nanoparticles alone. This results in uniform MoS_2 crystal with large area. At the same time, more and more MoO_3 powder evaporates and is sulfurated into MoS_2 by a series of reactions. The synthesized material adsorbs on the initially sulfurized MoS_2 region edges or central nucleation sites due to their higher reaction reactivity,[35] eventually forming large and continuous MoS_2 films. This is consistent with previous reports on growth of large-area monolayer MoS_2 films.[36–38] We also investigated the growth process and mechanism. The appearance and distribution of the reactive intermediate MoO_{3-x} play an essential role in synthesis of continuous large-area films due to its lowest saturation vapor density.

To evaluate the electronic properties of the as-grown MoS_2 films, back-gated FETs were fabricated on SiO_2/Si substrates using Ti/Au as source–drain (S–D) electrodes and a *p*-doped silicon substrate as the back gate without a transfer procedure, which could introduce contamination and/or degradation.[26] A schematic diagram of the fabricated FET is shown in Fig. 8a. A typical transfer and output characteristics of the MoS_2 FETs are shown in Fig. 8b and c. The drain–source current (I_{DS}) increased monotonically with increasing gate-to-source voltage (V_{GS}) at varied drain–source voltage (V_{DS}), indicating *n*-type semiconducting behavior. The on/off ratio was extracted from the log $I_{DS}-V_{GS}$ curves, being above 10^4. The SS of the MoS_2 FETs was estimated to be $\sim$ 0.44 V dec^{-1}. The electronic properties of such MoS_2-based FETs could be improved by use of high-*k* dielectrics and interface engineering.

CONCLUSIONS

Continuous monolayer large-area MoS_2 thin films were synthesized on SiO_2/Si substrate by CVD method, and the growth conditions optimized. The dimensions of the continuous MoS_2 films were on micron scale. Optical microscopy, Raman, PL, AFM, and SEM observations showed that the MoS_2 films were continuous monolayers with thickness $\sim$ 0.71 nm. XPS spectra demonstrated that the as-grown films had $\sim$ 1:2 Mo/S ratio. The FWHM of the Raman peaks confirmed the high quality of the MoS_2 films, comparable to exfoliated monolayers. HRTEM images revealed that the MoS_2 had single-crystal structure. Transistors fabricated using MoS_2 films showed typical field-effect characteristics with on/off ratio of $\sim 10^4$ and SS of $\sim$ 0.44 V dec^{-1}. Optical microscopy and SEM images revealed the morphological variation of the MoS_2 films after different reaction times, confirming a growth mechanism for MoS_2 in which the appearance and distribution of the reactive intermediate MoO_{3-x} contribute to synthesis of continuous large-area films due to its lowest saturation vapor density. The results of this work suggest an approach for controllable synthesis of large-area films required for future scale-up of MoS_2 device fabrication.

ACKNOWLEDGEMENTS

This work is supported by the National Natural Science Foundation of China (Grant No. 51472096), Fundamental Research Funds for the Central Universities (Grant No. 2017KFYXJJ041), and R&D Program of Ministry of Education of China (No. 62501040202). The authors would like to acknowledge the Analytical and Testing Center of Huazhong University of Science and Technology (HUST) for providing facilities for Raman, PL, XPS measurements, and HRTEM characterization. Finally, thanks are due for facility support from the Center for Nanoscale Characterization & Devices (CNCD), WNLO of HUST for carrying out scanning electron microscopy measurements.

REFERENCES

1. W. Bao, X. Cai, D. Kim, K. Sridhara, and M.S. Fuhrer, *Appl. Phys. Lett.* 102, 042104 (2013).
2. Y. Liu, L. Hao, W. Gao, Z. Wu, Y. Lin, G. Li, W. Guo, L. Yu, H. Zeng, J. Zhu, and W. Zhang, *Sens. Actuators B* 211, 537 (2015).
3. S. Lin, P. Wang, X. Li, Z. Wu, Z. Xu, S. Zhang, and W. Xu, *Appl. Phys. Lett.* 107, 153904 (2015).

4. L. Hao, Y. Liu, W. Gao, Y. Liu, Z. Han, L. Yu, Q. Xue, and J. Zhu, *J. Alloys Compd.* 682, 29 (2016).
5. I. Lahouij, E.W. Bucholz, B. Vacher, S.B. Sinnott, J.M. Martin, and F. Dassenoy, *Nanotechnology* 23, 375701 (2012).
6. X. Peng and R. Ahuja, *Nano Lett.* 8, 4464 (2008).
7. Y.C. Lin, W. Zhang, J.K. Huang, K.K. Liu, Y.H. Lee, C.T. Liang, C.W. Chu, and L.J. Li, *Nanoscale* 4, 6637 (2012).
8. Q.H. Wang, K.K. Zadeh, A. Kis, J.N. Coleman, and M.S. Strano, *Nat. Nanotechnol.* 7, 699 (2012).
9. J. Hong, C. Jin, J. Yuan, and Z. Zhang, *Adv. Mater.* 29, 1606434 (2017).
10. W. Wu, D. De, S.C. Chang, Y. Wang, H. Peng, J. Bao, and S.S. Pei, *Appl. Phys. Lett.* 102, 142106 (2013).
11. N. Perea-lopez, Z. Lin, N.R. Pradhan, A. Iniguez-rabago, A. Laura Elias, A. Mccreary, J. Lou, P.M. Ajayan, H. Terrones, L. Balicas, and M. Terrones, *2D Mater.* 1, 011004 (2014).
12. F.K. Perkins, A.L. Friedman, E. Cobas, P.M. Campbell, G.G. Jernigan, and B.T. Jonker, *Nano Lett.* 13, 668 (2013).
13. D. De Fazio, I. Goykhman, D. Yoon, M. Bruna, A. Eiden, S. Milana, U. Sassi, M. Barbone, D. Dumcenco, K. Marinov, A. Kis, and A.C. Ferrari, *ACS Nano* 10, 8252 (2016).
14. J. Zhao, W. Chen, J. Meng, H. Yu, M. Liao, J. Zhu, and R. Yang, *Adv. Electron. Mater.* 2, 3 (2016).
15. B. Radisavljevic, A. Radenovic, J. Brivio, V. Giacometti, and A. Kis, *Nat. Nanotechnol.* 6, 147 (2011).
16. A. Splendiani, L. Sun, Y. Zhang, T. Li, J. Kim, C.Y. Chim, G. Galli, and F. Wang, *Nano Lett.* 10, 1271 (2010).
17. L. Hao, Y. Liu, W. Gao, Z. Han, Q. Xue, H. Zeng, Z. Wu, J. Zhu, and W. Zhang, *J. Appl. Phys.* 117, 114502 (2015).
18. G. Eda, H. Yamaguchi, D. Voiry, T. Fujita, M. Chen, and M. Chhowalla, *Nano Lett.* 11, 5111 (2011).
19. Y.H. Lee, X.Q. Zhang, W. Zhang, M.T. Chang, C.T. Lin, K.D. Chang, Y.C. Yu, J.T. Wang, C.S. Chang, L.J. Li, and T.W. Lin, *Adv. Mater.* 24, 2320 (2012).
20. Y. Yu, C. Li, Y. Liu, L. Su, Y. Zhang, and L. Cao, *Sci. Rep.* 3, 1866 (2013).
21. C. Nie, L. Yu, X. Wei, J. Shen, W. Lu, W. Chen, S. Feng, and H. Shi, *Nanotechnology* 28, 275203 (2017).
22. A.M. van der Zande, P.Y. Huang, D.A. Chenet, T.C. Berkelbach, Y. You, G.-H. Lee, T.F. Heinz, D.R. Reichman, D.A. Muller, and J.C. Hone, *Nat. Mater.* 12, 554 (2013).
23. S. Najmaei, Z. Liu, W. Zhou, X. Zou, G. Shi, S. Lei, B.I. Yakobson, J. Idrobo, P.M. Ajayan, and J. Lou, *Nat. Mater.* 12, 754 (2013).
24. Y. Zhan, Z. Liu, S. Najmaei, P.M. Ajayan, and J. Lou, *Small* 8, 966 (2012).
25. D. Dumcenco, D. Ovchinnikov, K. Marinov, P. Lazić, M. Gibertini, N. Marzari, O. Lopez Sanchez, Y.-C. Kung, D. Krasnozhon, M.-W. Chen, S. Bertolazzi, P. Gillet, A. Fontcuberta i Morral, A. Radenovic, and A. Kis, *ACS Nano* 9, 4611 (2015).
26. T.J. Marks and M.C. Hersam, *Nature* 520, 631 (2015).
27. S. Lin, X. Li, P. Wang, Z. Xu, S. Zhang, H. Zhong, Z. Wu, W. Xu, and H. Chen, *Sci. Rep.* 5, 15103 (2015).
28. M.R. Laskar, L. Ma, S. Kannappan, P.S. Park, S. Krishnamoorthy, D.N. Nath, W. Lu, Y. Wu, and S. Rajan, *Appl. Phys. Lett.* 102, 252108 (2013).
29. G. Eda, H. Yamaguchi, D. Voiry, T. Fujita, M. Chen, and M. Chhowalla, *Nano Lett.* 11, 5111 (2011).
30. C. Lee, H. Yan, L.E. Brus, T.F. Heinz, J. Hone, and S. Ryu, *ACS Nano* 4, 2695 (2010).
31. R.F. Frindt, *J. Appl. Phys.* 37, 1928 (1966).
32. K. Liu, W. Zhang, Y. Lee, Y. Lin, M. Chang, C. Su, C. Chang, H. Li, Y. Shi, H. Zhang, C. Lai, and L. Li, *Nano Lett.* 12, 1538 (2012).
33. M.A. Baker, R. Gilmore, C. Lenardi, and W. Gissler, *Appl. Surf. Sci.* 150, 255 (1999).
34. X.L. Li and Y.D. Li, *Chem. Eur. J.* 9, 2726 (2003).
35. T. Liang, S. Xie, Z. Huang, W. Fu, Y. Cai, X. Yang, H. Chen, X. Ma, H. Iwai, D. Fujita, N. Hanagata, and M. Xu, *Adv. Mater. Interfaces* 4, 1600687 (2016).
36. X. Yang, Q. Li, G. Hu, Z. Wang, Z. Yang, X. Liu, M. Dong, and C. Pan, *Sci. China Mater.* 59, 182 (2016).
37. J. Chen, W. Tang, B. Tian, B. Liu, X. Zhao, Y. Liu, T. Ren, W. Liu, D. Geng, H.Y. Jeong, H.S. Shin, W. Zhou, and K.P. Loh, *Adv. Sci.* 3, 8 (2016).
38. S. Wang, Y. Rong, Y. Fan, M. Pacios, H. Bhaskaran, K. He, and J.H. Warner, *Chem. Mater.* 26, 6371 (2014).